A Scalable Model for Silicon Spiral Inductors

Angelo Scuderi, Tonio Biondi, Egidio Ragonese, and Giuseppe Palmisano

Università di Catania, Facoltà di Ingegneria, DIEES, V.le A. Doria 6, 95125 Catania, Italia
E-mail: ascuderi@diees.unict.it, tbiondi@diees.unict.it, eragone@diees.unict.it, gpalmisano@diees.unict.it

***Abstract* — A simple model for monolithic spiral inductors on silicon substrate is presented. Each lumped element of the model is related to the layout geometry by analytical equations. Moreover, a novel equation for series resistance is also proposed. The model was validated by comparisons with on-wafer measurements over a wide range of geometrical layout parameters.**

I. Introduction

Spiral inductors are widely used to improve the performance of transceiver circuit blocks such as low noise amplifiers (LNAs), voltage controlled oscillators (VCOs), intermatching networks and RF filters.

Unfortunately, metal and substrate loss mechanisms limit the quality factor of such devices. At higher frequencies, the series resistance of the metallization increases due to skin and crowding effects, while magnetically induced currents flow into the highly-conductive substrate. Many authors have proposed layout optimizations to obtain inductors with higher quality factors [1]. The realization of a patterned ground shield (PGS) has proved to be useful in reducing the magnetically induced currents in the low-resistance substrate underlying the spiral.

Modeling all loss phenomena is a hard task and only EM simulators can provide an accurate estimation of inductor performance parameters over a wide frequency range. Two different methodologies to extract inductor models are commonly adopted in literature: distributed equivalent networks [2] and compact π-models [3]. In the first approach, each turn is modeled by a π-network and then all these networks are coupled together. This model can approximate the device performance very well, but it is quite difficult to manage for RF designers. In contrast, compact π-models are quite simple and allow accurate prediction of the self-resonance effects of monolithic inductors. A frequency-dependent series resistance is commonly used to estimate quality factor at higher frequencies. Numeric methods, fitting parameters or complex equations are implemented to obtain good agreement with experimental data over a wide range of geometries.

This paper discusses a model that takes into account all loss phenomena with simple analytical equations related to inductor geometry. A new empirical equation for the series resistance is formulated and its parameters are extracted from measurements. The model is scalable over a wide range of inductor geometries and shows excellent agreement with experimental data up to the self-resonance frequency.

TABLE I
CLASSIFICATION OF INDUCTORS

Type	W	Din	Type	W	Din	Type	W	Din
A	6	50	G	14	50	O	20	50
B	6	100	H	14	100	P	20	100
C	6	150	I	14	150	Q	20	150
D	10	50	L	18	50			
E	10	100	M	18	100			
F	10	150	N	18	150			

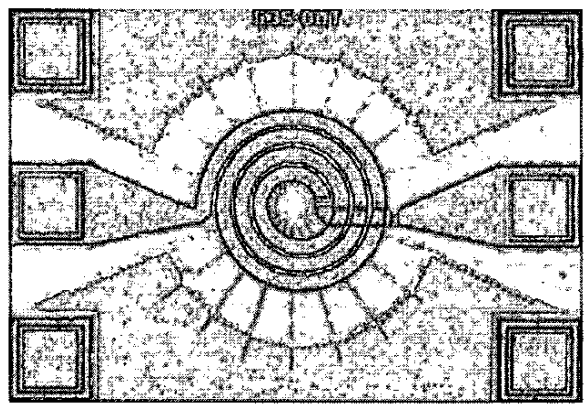

Fig. 1. Die photograph of the integrated inductor G35

II. Integrated Inductors

A high-speed bipolar technology supplied by STMicroelectronics, Catania, was used to integrate a wide series of single-layer circular inductors. The process provides three metallization layers: the spiral is fabricated using the top metal layer (with the lowest sheet resistance), while the underpass and the ground metal plane use the second and first layers, respectively. A PGS is realized with the highly-doped buried layer required by bipolar transistors by means of a radial oxide trench pattern.

0-7803-7695-1/03/$17.00 © 2003 IEEE

Substrate n^+ sinkers contact each circular sector of the shield to the metal ground plane. The PGS geometry and the distance between the spiral and ground plane were optimized by means of 3D EM simulations.

Integrated inductors were classified into 15 types: their width (W) and inner diameter (Din) are reported (in μm) in table I. Each type has the following numbers of turns: 2.5, 3.5, 4.5, and 5.5. In the following each inductor will be identified with the type followed by the number of turns. The spacing between adjacent turns and the distance between the spiral and ground metal plane were set to 4 μm and 50 μm, respectively. A photograph of an integrated inductor is shown in Fig. 1.

For each inductor, de-embedding structures were fabricated to eliminate layout test pattern parasitics. All these devices were characterized up to 20 GHz by two-port *S*-parameter measurements.

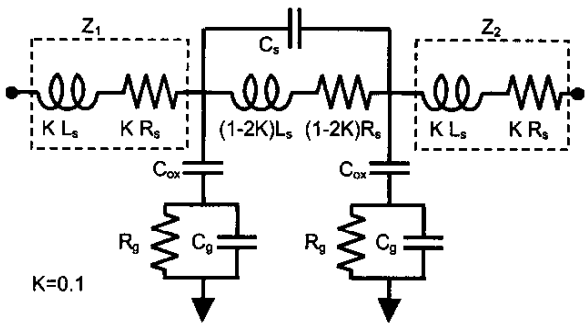

Fig. 2. Lumped model for planar inductors on PGS.

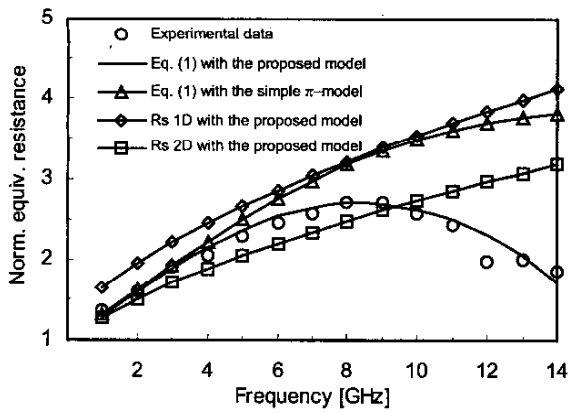

Fig. 3. Simulated and measured normalized equivalent series resistance.

II. Model Description

The proposed model is shown in Fig. 2. It approximates more closely a distributed network than the traditional π-model, but it maintains the advantages of simplicity. Indeed, simulations showed that by adding impedances Z_1 and Z_2 to the standard π-model, a more accurate prediction of *Y* and *S* parameters are achieved. The standard π-model is able to approximate inductance ($L = \mathrm{Imag}(1/Y_{11})/\omega$) and the quality factor ($Q = -\mathrm{Imag}(Y_{11})/\mathrm{Real}(Y_{11})$) as well, but it does not take into account the Y_{12} parameter properly.

The experimental measurement of the real part of $-1/Y_{12}$ provides the series resistance at frequency lower than the peak quality factor frequency. The series losses in the spiral are modeled by component R_s, which is quite difficult to estimate due to AC rise caused by skin and crowding effects. However accurate model of R_s is the key point for the prediction of the quality factor. It is worth noting that, due to the magnetic coupling between adjacent turns, the frequency dependence of the series resistance is not fully described by the square root law of the skin effect. As a consequence, an empirical law was formulated and its parameters were extracted from experimental measurements:

$$R_s = R_{DC}\frac{1+\frac{f}{f_0}+\left(\frac{1.7f}{SRF}\right)^2}{1+\left(\frac{f}{SRF}\right)^2} \qquad (1)$$

where R_{DC} is the DC resistance of the metal, SRF is the self-resonance frequency $1/\left(2\pi\sqrt{L_s C_{ox}}\right)$. The value of f_0 was set to 7 and 3.5 GHz for 6 and 10 μm widths, respectively. It was set to 2.8 GHz for 14, 18 and 20 μm widths. The classical one- and two-dimensional approximations of R_s including skin depth [4] are reported in equations (2), respectively:

$$R_{s1D} = R_{DC}\frac{t}{\delta(1-e^{-t/\delta})} \text{ and } R_{s2D} = R_{s1D}\frac{1}{(1+\frac{t}{W})} \qquad (2)$$

where t is the metal thickness and δ is the skin depth. Equations (1) and (2) were used with the proposed model and the simple π-model to compare the accuracy with respect to measured data. The simulated and measured equivalent series resistances, normalized with respect to the DC value, are shown in Fig. 3. It is clear that equation (1) in the proposed model provides the best fit to measured data.

In the proposed model, component L_s represents the inductive behavior whose value can be calculated by using any formula reported in literature. In this paper, the current sheet approximation [5] is used.

The substrate effects are modeled by two oxide capacitances (C_{ox}), in series with RC networks that model the PGS. It is well known that the displacement of charge

between the spiral and the buried layer determines capacitive effects that have a large impact on self-resonance frequency and the quality factor. The value of C_{ox} arises from both the area (C_a) and perimeter (C_p) effects and can easily be estimated with the following equations:

$$C_a = A\frac{\varepsilon_{ox}}{t_{ox}} \quad \text{and} \quad C_P = PC_{sp} \tag{3}$$

$$C_{ox} = \frac{1}{2}(C_a + C_P) \tag{4}$$

where A is the area of the spiral, P is the length of its inner and outer circumference, C_{sp} is a unit-length specific capacitance, ε_{ox} and t_{ox} are the dielectric constant and the oxide thickness, respectively. Since in bipolar processes several planarization steps occur, the oxide thickness may be slightly different from the nominal values due to process tolerances. The correct value of t_{ox} was extracted from experimental measurements, reported in Fig. 4. 3D EM simulations, performed with Ansoft HFSS, confirmed its accuracy. Indeed, the 3D EM simulator showed excellent agreement with all experimental measurements up to frequencies well above self-resonance. The simulated constant E-field contours between the spiral and the substrate show that the main capacitive contribution is due to the area and the inner and outer perimeter of the spiral, as shown in Fig. 5. The electrical coupling between adjacent turns has indeed negligible effects. The capacitive effect due to overlap between the spiral and underpass is modeled by capacitor C_s whose value is calculated by equation (3), where t_{ox} and C_{sp} are the thickness and the unit-length specific capacitance between the spiral and underpass, respectively.

A RC network can easily model the PGS. The value of resistance R_g comes from the geometry and size of each circular sector according to the following equation:

$$R_g = \frac{1}{N_{set}}\frac{R_{sheet}L_{PGS}}{W_{PGS}} \tag{5}$$

where R_{sheet} is the buried layer sheet resistance, N_{set} is the PGS sector number and L_{PGS} and W_{PGS} are the length and width of each sector. Capacitor C_g is calculated by using the well-known silicon time constant formula, $RC = \rho_{Si}\cdot\varepsilon_{Si}$ where ρ_{Si} and ε_{Si} are the resistivity and dielectric permittivity of the buried layer.

III. Model Validation

The model was validated by comparison with the fully de-embedded two port measurements of the inductors described in section I. Figs. 6 and 7 show the excellent

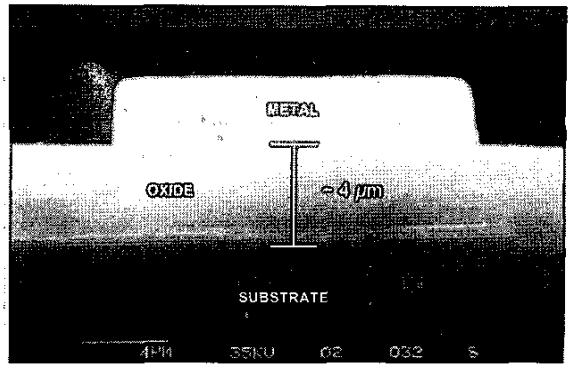

Fig. 4. SEM cross-section of an integrated inductor.

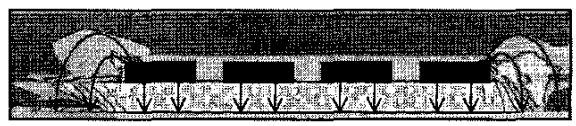

Fig. 5. Constant E-field contours simulated by HFSS.

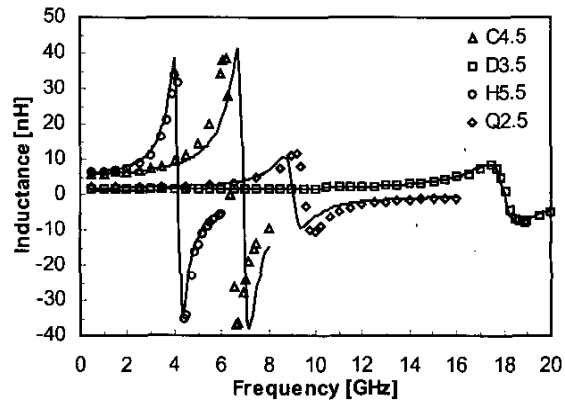

Fig. 6. Comparison between simulated (continuous line) and measured (symbols) inductance.

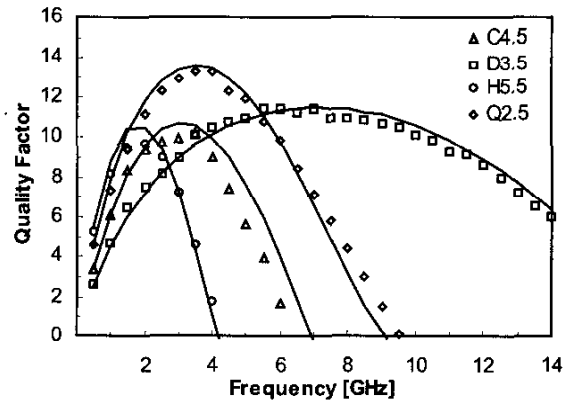

Fig. 7. Comparison between simulated (continuous line) and measured (symbols) quality factor.

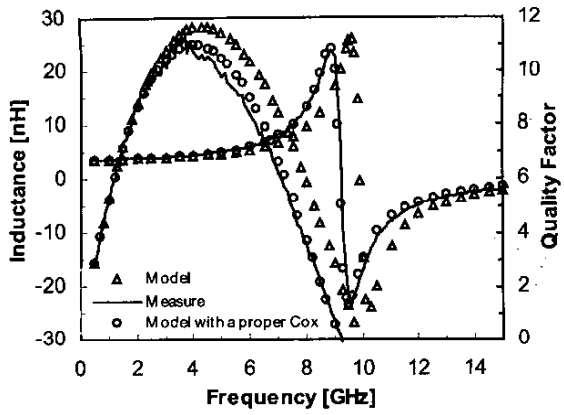

Fig. 8. Effects of C_{ox} on simulated inductance and quality factor for inductor B4.5.

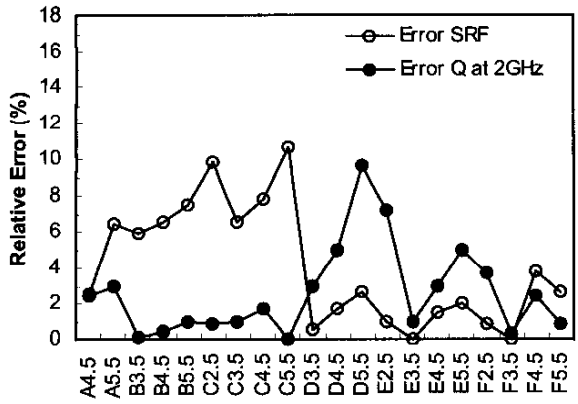

Fig. 9. Relative error of SRF and quality factor at 2 GHz.

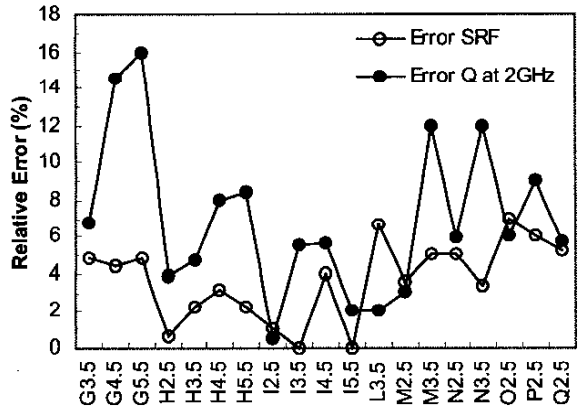

Fig. 10. Relative error of SRF and quality factor at 2 GHz.

agreement obtained by the model up to frequencies above self-resonance.

The geometrical formula for C_{ox} reveals errors for $W = 6\ \mu m$, which leads to an overestimated SRF and Q-factor owing to equation (3). Using a proper C_{ox} value extracted from measurements allows both of them to be simulated accurately, as shown in Fig. 8, which confirms the validity of equation (1). However additional fitting parameters need to be added to equation (3) to achieve higher accuracy thus losing the physics-based nature of the model.

Figs. 9 and 10 report the relative errors of the proposed model for all considered inductors. The self-resonance frequency was estimated to have less than 10% errors while the quality factor at 2 GHz presented a relative error of approximately 10% with a peak of 16% for the G5.5 inductor. Integrated inductors with measured self-resonance frequency exceeding 20 GHz were not considered.

V. Conclusion

A lumped model for monolithic inductors on silicon substrate has been presented. It has an improved π topology and includes a novel equation for series resistance. Model components were related to inductor layout geometry by means of analytical equations reducing the number of fitting parameters to only one. Despite its simple topology, the model is able to predict the performance parameters of a wide range of integrated inductors up to the self-resonance frequency.

Acknowledgements

This work was supported by the IST project "PERLA" of EU.

References

[1] C. P. Yue, and S. S. Wong, "On-Chip Spiral Inductors with Pattened Ground Shields for Si-Based RFIC's," *IEEE J. Solid State Circuits*, vol. 33, no. 5, pp. 743-752, May 1999.

[2] J. R. Long, and M. A. Copeland, "The Modeling, Characterization, and Design of Monolitic Inductors for Silicon RF IC's," *IEEE J. Solid State Circuits.*, vol. 32, no. 3, pp. 357-368, March 1997.

[3] C. P. Yue, and S. S. Wong, "Physical Modeling of Spiral Inductors on Silicon," *IEEE Trans. On Electron Devices.*, vol. 47, no. 3, pp. 560-568, March 2000.

[4] Y. Eo, and W. R. Eisenstadt, "High-Speed VLSI Interconnect Modeling Based on S-Parameter Measurements," *IEEE Trans. On Components, Hybrids, and Manufacturing.*, vol. 16, no. 5, pp. 555-562, August 1993.

[5] S. S. Mohan, M. del Mar Hershenson, S. P. Boyd, and T. H. Lee, "Simple Accurate Expression for Planar Spiral Inductances," *IEEE J. Solid State Circuits*, vol. 34, no. 10, pp. 1419-1424, Oct 1999.